International Journal of Minerals, Metallurgy and Materials
Volume 30, Number 2, February 2023, Page 354
https://doi.org/10.1007/s12613-022-2548-7

Kinetics of austenite growth and bainite transformation during reheating and cooling treatments of high strength microalloyed steel produced by sub-rapid solidification

Wanlin Wang[1,2], *Lankun Wang*[1,2], *and Peisheng Lyu*[1,2]✉

1) School of Metallurgy and Environment, Central South University, Changsha 410083, China
2) National Center for International Research of Clean Metallurgy, Central South University, Changsha 410083, China
(Received: 7 July 2022; revised: 7 September 2022; accepted: 8 September 2022)

Abstract: First, strip cast samples of high strength microalloyed steel with sub-rapid solidification characteristics were prepared by simulated strip casting technique. Next, the isothermal growth of austenite grain during the reheating treatment of strip casts was observed *in situ* through confocal laser scanning microscope (CLSM). The results indicated that the time exponent of grains growth suddenly rise when the isothermal temperature higher than 1000°C. And the activation energy for austenite grain growth were calculated to be 538.0 kJ/mol in the high temperature region (above 1000°C) and 693.2 kJ/mol in the low temperature region (below 1000°C), respectively. Then, the kinetics model of austenite isothermal growth was established, which can predict the austenite grain size during isothermal hold very well. Besides, high density of second phase particles with small size was found during the isothermal hold at the low temperature region, leading to the refinement of austenite grain. After isothermal hold at different temperature for 1800 s, the bainite transformation in microalloyed steel strip was also observed *in situ* during the continuous cooling process. And growth rates of bainite plates with different nucleation positions and different prior austenite grain size (PAGS) were calculated. It was indicated that the growth rate of the bainite plate is not only related to the nucleation position but also to the PAGS.

Keywords: microalloyed steel; strip casting; precipitation; austenite growth; bainite transformation

1. Introduction

In recent years, high strength steels have received wide attention to achieve the goal of automobile lightweight, which is the development trend in automobile industry. Among them, high strength microalloyed steels is considered to have a good application prospect because of their low alloy cost, excellent combination of strength and ductility [1–5]. At present, the main casting methods of high strength microalloyed steels are conventional continuous casting (CCC) and compact strip production (CSP) [6–8]. However, a lot of rolling processes are needed to produce the hot rolled strip by these two production methods, leading to high pollution and high energy consumption.

Unlike CCC and CSP technology, strip casting technology can directly cast the molten steel into the steel strip with thickness of several millimeters followed by single pass hot rolling (rolling reduction below 30%) to obtain final strip product [9–10]. The production line of strip casting to produce hot rolled strip are greatly simplified since it integrates the processes of casting and rolling [11–14]. Due to the rapid solidification process of molten steel and the elimination of a large amount of processing stages like hot rolling, strip casting technology possesses many advantages, such as emission reduction, energy saving, and low operating and investment costs, and the strip cast production has sub-rapid solidification characteristics [15–16]. Therefore, strip casting has attracted extensive attention from researchers all over the world. At present, twin-roll strip casting (TRSC) is the most popular strip casting technology for steel strip production, and it has been successfully used in steel industry for the production of plain carbon steel, low-carbon microalloyed steel ($\omega_C < 0.1$wt%, ω_C represents the mass percent of element C), silicon steel, and stainless steel [9–10]. To explore the feasibility of producing advanced high strength steels by strip casting, some researchers have done many fundamental studies on the strip casting of dual phase (DP) steel, transformation-induced plasticity (TRIP) steel, and twinning-induced plasticity (TWIP) steel using pilot-scale strip caster or lab-scale strip-casting simulator [17–22]. It has been demonstrated that the steel strip produced directly by strip casting without any hot rolling or heat treatment owns a lower strength than that produced by conventional methods [18]. Consequently, extra thermomechanical treatments of the steel strip produced directly by strip casting were applied to achieve a better combination of strength and ductility. For example, Xiong *et al.*

✉ Corresponding author: Peisheng Lyu E-mail: Lyu.peisheng@csu.edu.cn

[17,20] improved the comprehensive mechanical properties of DP and TRIP steel strips by using hot rolling. Shrestha *et al.* [23] and Xie *et al.* [24] enhanced the strength of low-carbon microalloyed steel strip without loss in ductility through the formation of clusters induced by aging treatment.

Austenization is often applied in hot rolled low-carbon steels produced by conventional casting to obtain finer austenite grains and final microstructure, and therefore a better combination of strength and ductility can be achieved [25–30]. Besides, the kinetics of austenite isothermal growth and bainite transformation during reheating and cooling processes of the steels produced by conventional casting was also studied widely [31–35]. However, the austenite isothermal growth and bainite transformation during the reheating and continuous cooling processes of the steels with sub-rapid solidification characteristics which was produced by strip casting have not been studied yet. In our previous study [36–37], the strip casting of high strength microalloyed steel (ω_C = 0.2wt%) was simulated to investigate the interfacial heat transfer and the microstructure and mechanical properties of strip cast without extra thermomechanical treatments. In this study, confocal laser scanning microscope (CLSM) was used to *in situ* observe the austenite isothermal growth of the high strength microalloyed steel produced by simulated strip casting at different holding temperatures and to *in situ* observe the bainite transformation during continuous cooling after isothermal hold for 1800 s. Then, the kinetics of austenite isothermal growth and bainite transformation was investigated.

2. Experimental

The chemical composition of investigated steel was shown in Table 1. The strip cast samples used in this study were obtained by strip-casting simulator in the Steel Research Center at Central South University, China, as shown in Fig. 1. In our previous study, it has been demonstrated that this strip-casting simulator can simulate the strip casting of steel well [37–38]. Fig. 2 shows the experiment process of the strip-casting simulator. At first, 5 kg experimental steel was put into the crucible and heated to 1560°C by induction furnace under the protection of high purity argon atmosphere (Fig. 2(a)). Through proportion integration differentiation (PID) control technique, temperature of experimental steel was ensured to be 1560°C until the experiment completed. Next, the copper substrate was immersed into the molten steel at the speed of 0.7 m/s and stayed in the molten bath for 350 ms (Fig. 2(b)). Then, the copper substrate with strip cast formed by sub-rapid solidification was withdrawn to original position (Fig. 2(c)). And the microstructure of the strip cast was proved to be bainite ferrite (BF) and acicular ferrite (AF) mainly by optical microscope. In the end of strip-casting simulation experiment, the air-cooled strip cast with the dimension of 30 mm × 40 mm × 1 mm (Fig. 3(a)) was removed from copper substrate. During the whole experiment process, high-purity argon gas was used for protecting furnace chamber.

Table 1. Chemical composition of studied microalloyed steel

wt%

C	Si	Mn	Ti	Mo	Cu	Nb	Fe
0.20	0.25	1.4	0.02	0.15	0.01	0.04	Bal.

In order to *in situ* observe the austenite grain isothermal growth and bainite transformation by confocal laser scanning microscope (CLSM, VL2000DX-SVF18SP), strip casts produced by strip casting simulation were machined into cuboid samples with the dimension of 4 mm × 1 mm × 3 mm (Fig. 3(b)). The cross section of cuboid samples was selected as the observation surface after being polished. The temperature history during the reheating and cooling treatment of strip cast samples using CLSM was shown in Fig. 3(c). During the CLSM experiment, samples were heated to a certain holding temperature (850 to 1350°C) with a heating rate of 15°C/s. After isothermal hold for 1800 s, the samples were continuously cooled to room temperature at the rate of 30°C/s.

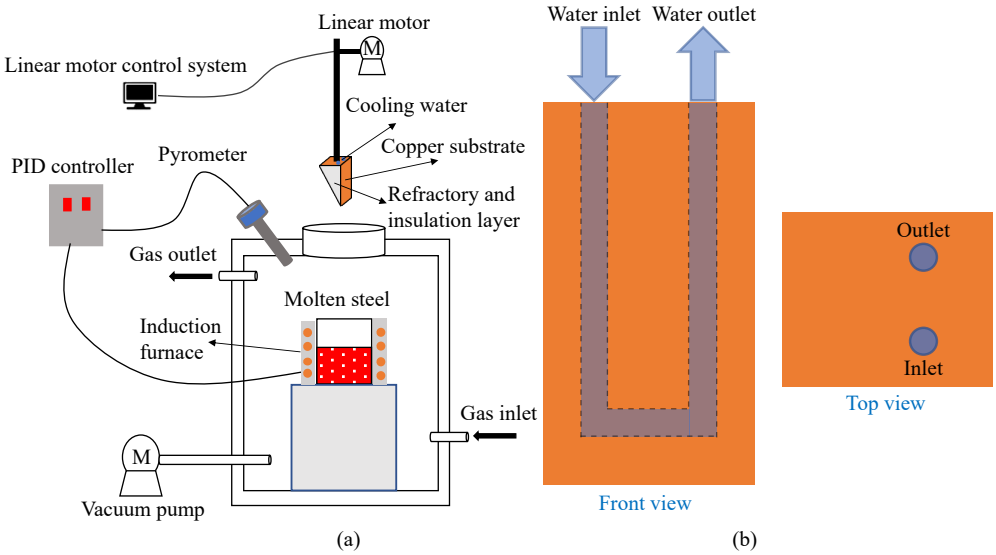

Fig. 1. Schematic illustration of (a) strip-casting simulator and (b) copper substrate.

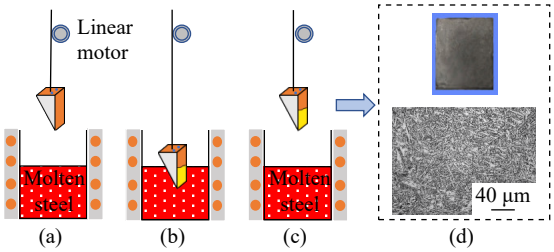

Fig. 2. Experimental process of strip-casting simulation: (a) molten steel at target temperature, (b) immersion of the copper substrate and stay for a certain time, and (c) quick withdrawal of the copper substrate. (d) Obtained strip cast sample (top) and its microstructure image (bottom).

High purity argon gas was used to protect the samples from being oxidized during the *in-situ* observation. Charge-couple device (CCD) camera was used to record the microstructure evolution during CLSM experiment at the rate of 5 frames per second. ImageJ and Photoshop were used for calculating the austenite grain size and the length of bainite plate. For the transmission electron microscope (TEM, Talos F200X) observation of second phase particles in steel samples, the strip cast samples were reheated to 970 and 1050°C, respectively, using muffle furnace with a heating rate of 15°C/s, then were water quenched after holding for 1800 s in order to retain the second phase particles formed at holding temperature. Foil samples for TEM observation were prepared by Ion beam thinner (IBT, Gatan691). In this study, the thermodynamic software (FactSage 7.2) was also employed to calculate the possible second phase particles of the studied steel.

3. Results and discussion

3.1. Isothermal growth of austenite grain

The isothermal growth process of austenite grain for the sample held at 1150°C was recorded by CLSM, as shown in Fig. 4. With the increasing of holding time, the austenite grains grew gradually and slight trace from previous grain boundaries can be observed. Fig. 5 shows the austenite grains of the samples held at different temperature for 1800 s. It can be found that the effect of holding temperature on austenite grain size is not obvious when the holding temperature is lower than 1000°C.

Fig. 6 shows the austenite grain size of the strip cast samples held at different temperatures for 1, 10, 100, and 1800 s. It has been reported in our previous study that the prior austenite grain size (PAGS) of strip cast for the studied microalloyed steel was approximately 80–300 μm [37]. It is indicated that the short-time reheating treatment below 1000°C can effectively refine the PAGS of the strip cast, which is beneficial to the refinement of the final microstructure and thus to the improve the final mechanical properties. Compared with the PAGS of the strip cast without reheating treatment, the PAGS distribution of the strip cast after reheating treatment is more uniform, which is consistent with the result reported by Daamen *et al*. [22].

The kinetics model of austenite grain isothermal growth can be expressed by the following equation [33]:

$$D^{1/n} - D_0^{1/n} = Kt \tag{1}$$

where K is rate constant, n is time exponent, t is holding time, D is average austenite grain size, and D_0 represents the austenite grain size at $t = 0$. It is noted that the simple model of austenite grain isothermal growth is widely used for the calculation of time exponent n [33,39]:

$$D^{1/n} = Kt \tag{2}$$

The logarithmic plot of austenite grain size versus holding time was shown in Fig. 7. It can be seen that the slope of the logarithmic plot can be divided into two groups: high temperature region with high slope and low temperature region with low slope. According to Eq. (2), the time exponent at different holding temperature is equal to the slopes of the lines shown in Fig. 7. The time exponents are shown in Fig. 8, which suggested that the time exponents n suddenly rise when isothermal temperature higher than 1000°C. Besides, n rose slowly with the increasing temperature when the holding temperature is below 1000°C and remained relatively stable when the holding temperature is higher than 1000°C. In order to simplify calculation, the average time exponent n was calculated to be (0.06 ± 0.015) in low temperature region (below 1000°C) and (0.22 ± 0.015) in high temperature region (above 1000°C). The time exponent in this study is far lower than the theoretical time exponent value of 0.5 for high pure metal [40–41], because the solute dragging of solute atoms and the pinning force of second phase particles for the studied microalloyed steel can hinder the movement of austenite boundary effectively. Fig. 9(a) shows the equilibrium phase diagram of the second phase particles

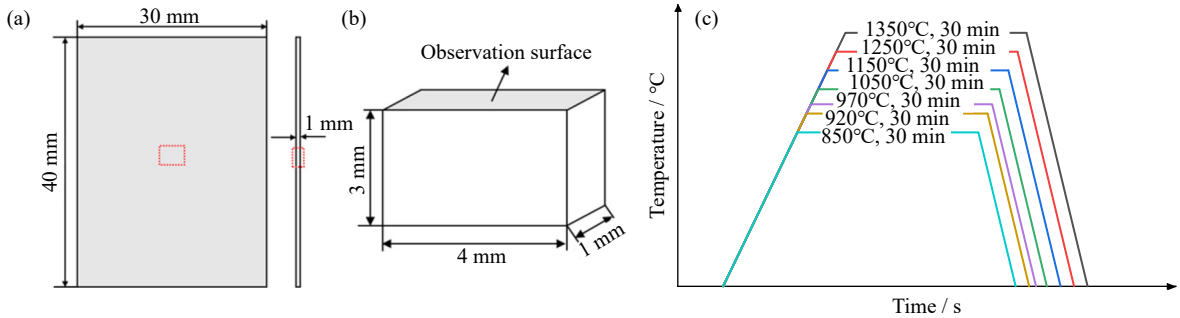

Fig. 3. Schematic diagrams of (a) the strip cast sample obtained by strip-casting simulator, (b) the cross section of samples from strip cast for *in-situ* observation, and (c) the temperature history for the heat treatment of strip cast samples using CLSM.

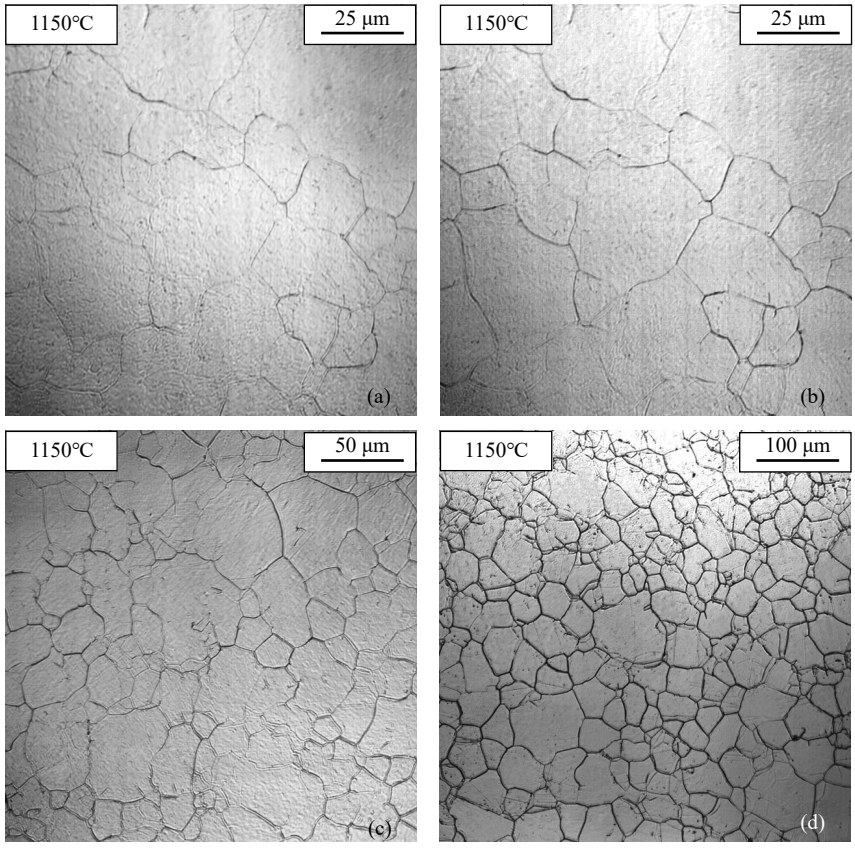

Fig. 4. ***In-situ*** **observation of the strip cast sample held at 1150°C for (a) 1 s, (b) 10 s, (c) 100 s, and (d) 1800 s.**

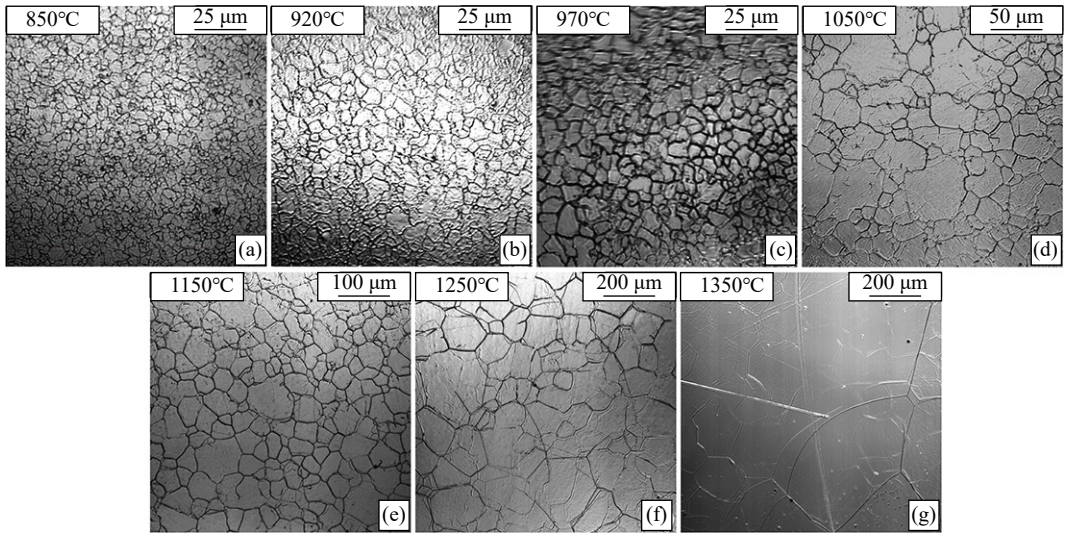

Fig. 5. Austenite grains of the strip cast samples held at 850 (a), 920 (b), 970 (c), 1050 (d), 1150 (e), 1250 (f), and 1350°C (g) for 1800 s.

in the studied steel by Factsage. It can be seen that the second phase particles between 700 to 1300°C are mainly carbides (TiC and NbC). It has been reported that the cooling rate has a great influence on the size and number density of the second phase particles in steel [42–43]. Compared to the steel strip produced by CCC or CSP processes, the steel strip produced by strip casting is more difficult to precipitate carbides because of the rapid cooling rate during secondary cooling process [37]. However, second phase particles would precipitate during the isothermal hold of strip cast according to the equilibrium phase diagram (Fig. 9(a)). In order to identify the second phase particles, TEM examination was conducted on the water-quenched strip cast samples after isothermal hold at 970°C (low temperature region) and 1050°C (high temperature region) for 1800 s. Fig. 9(b) and (c) shows the bright-field (BF) images of the second phase particles, from which it could be observed that the second phase particles with a smaller size and higher number density precipitated during the isothermal hold at the low temperature region compared to the high temperature region.

The pining force F of second phase particles can be calculated as follows [33]:

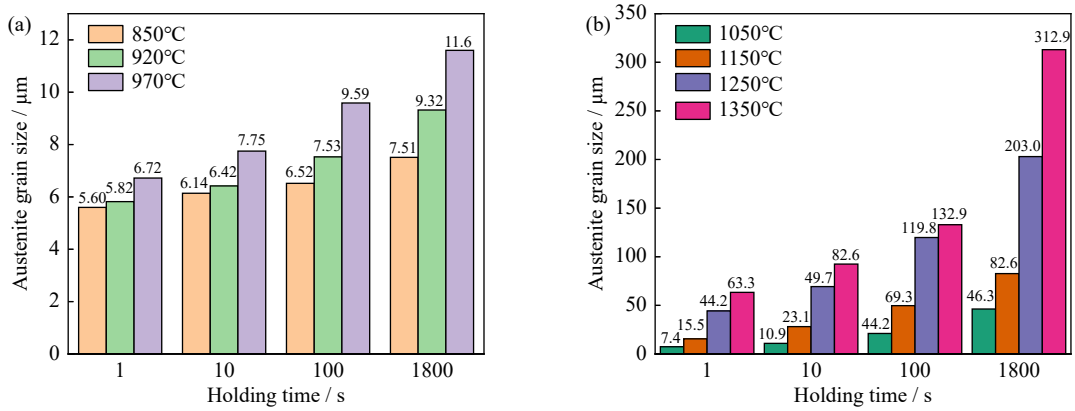

Fig. 6. Relationship between austenite grain size and holding time under different holding temperatures: (a) 850, 920, and 970°C; (b) 1050, 1150, 1250, and 1350°C.

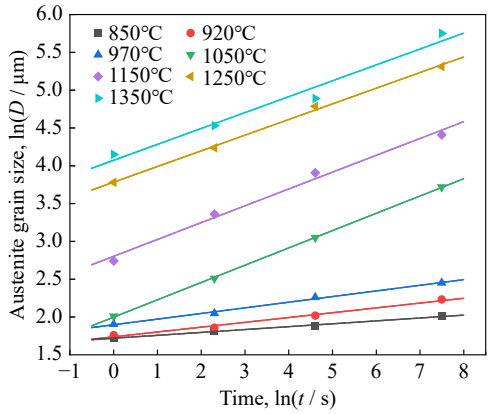

Fig. 7. Logarithmic graph of austenite grain size and holding time.

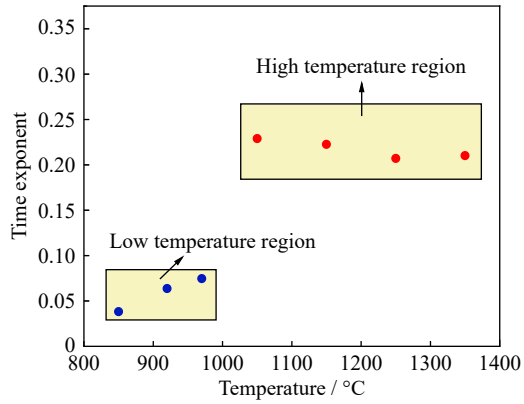

Fig. 8. Variation of time exponent with isothermal temperature.

$$F = c\gamma\frac{f}{r} \tag{3}$$

where c is constant, γ is grain boundary interfacial energy, and f and r are volume fraction and radius of particles, respectively. According to Eq. (3), the pinning force of second phase particles on austenite boundary during the isothermal hold at the low temperature region is higher than the high temperature region. Consequently, austenite grain grew slowly and became more refined in the low temperature region, which results in a lower time exponent in the low temperature region than in the high temperature region.

The rate of atomic diffusion is an important factor for hindering secondary phase particles growth in the lower temperature. The rate of atomic diffusion rises with the increase of the holding temperature. So, the radius of second phase particles increased with the rise of holding temperature, which results in the decrease of the pining force. According the previous study, the value of time exponent n was also considered to be related to the pinning force from second phase particles [33]. Therefore, the value of n rises slowly with temperature in the low temperature region. With the increase of the rate of atomic diffusion, the secondary phase particles precipitate completely at about 1000°C, which result in the suddenly rising of n in the Fig. 8.

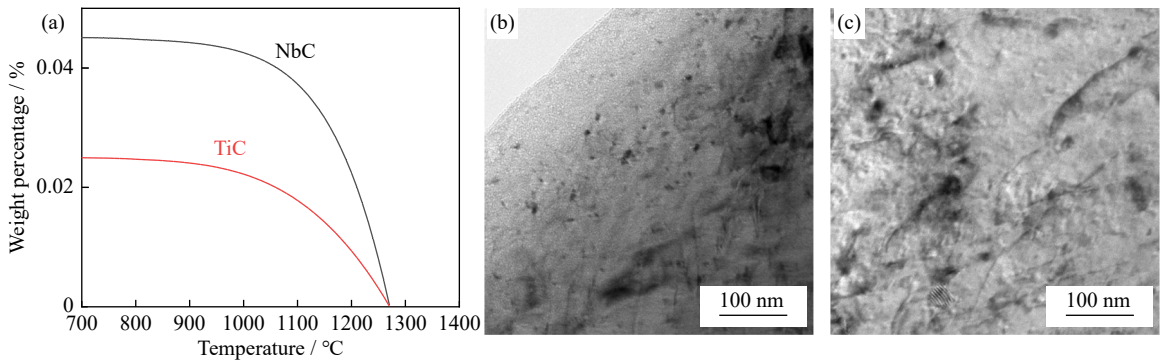

Fig. 9. (a) Equilibrium phase diagram of the second phase particles in studied steel by Factsage software; TEM BF images of the second phase particles the water-quenched strip samples after isothermal hold at 970°C (b) and 1050°C (c) for 1800 s.

The value of rate constant K in the different temperature can be obtained by the slope from the plot of $D^{1/n} - D_0^{1/n}$ versus t according to Eq. (1). The relationship between K and activation energy for austenite grain growth in the steel can be expressed by the following equation [33,39]:

$$K = A\exp(\frac{-Q}{RT}) \tag{4}$$

where A is material constant, Q is activation energy, R is gas constant, and T is holding temperature (Kelvin temperature). In order to calculate the activation energy, the relationship of ln K and $-1/(RT)$ in the low temperature region and high temperature region is plotted in Fig. 10. It can be obtained from Fig. 10 that the activation energy for austenite grain growth during the isothermal hold of strip cast samples is 538.0 kJ/mol in high temperature region (above 1000°C), and 693.2 kJ/mol in low temperature region (below 1000°C), respectively. Obviously, the activation energy for the austenite growth in different temperature regions are higher than the activation energy for the diffusion of elements in γ-Fe [31,44]. This is mainly due to the fact that the formation of (Nb,Ti)C particles prevents the migration of austenite grain boundary and thus increase the activation energy for the austenite growth. Besides, the solute elements also increase the activation energy for austenite grain growth by solute-drag effect [45]. It also can be seen that the growth resistance of grains in the high strength microalloyed steel produced by sub-rapid solidification is higher when the temperature is below 1000°C. Therefore, it is indicated that the reheating temperature selected for actual strip casting production should be below 1000°C for avoiding the coarsening of austenite grains. A higher activation energy in the low temperature region can be attributed to the evident pining effect during isothermal hold.

Furthermore, the kinetics model of austenite isothermal growth can be deduced as:

$$D^{1/0.06} - D_0^{1/0.06} = 3.001\times10^{43}\exp\left(-6.932\times\frac{10^5}{RT}\right)t \quad (T < 1273\ \text{K}) \tag{5}$$

$$D^{1/0.22} - D_0^{1/0.22} = 2.996\times10^{25}\exp\left(-5.38\times\frac{10^5}{RT}\right)t \quad (T \geq 1273\ \text{K}) \tag{6}$$

Fig. 11 compared the measured austenite grain size with the calculated austenite grain size using the above kinetics model, which shows the agreement between the experiment measurement and calculation. It can be concluded that the model established in this study can effectively reflect the kinetics of isothermal austenite growth of the studied microalloyed steel produced by strip casting process.

3.2. Kinetics of bainite transformation

The bainite starting temperature (B_s,°C) and martensite starting temperature (M_s,°C) of steels can be calculated ac-

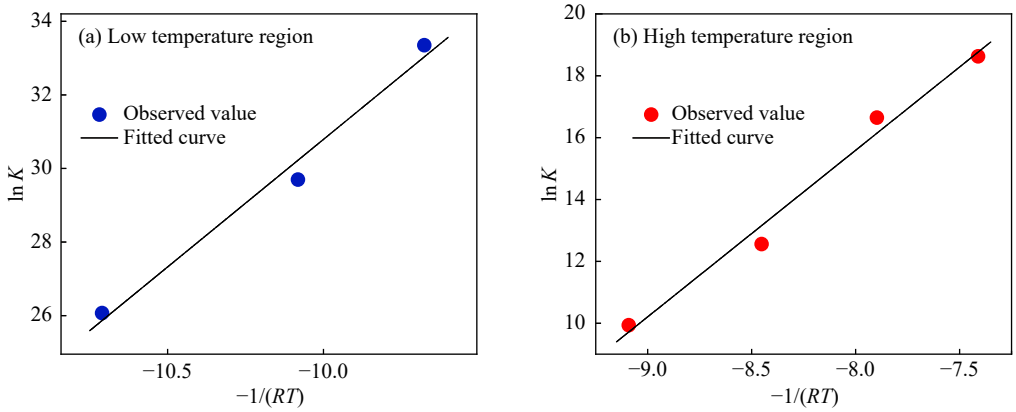

Fig. 10. Arrhenius-plot in (a) low temperature region and (b) high temperature region.

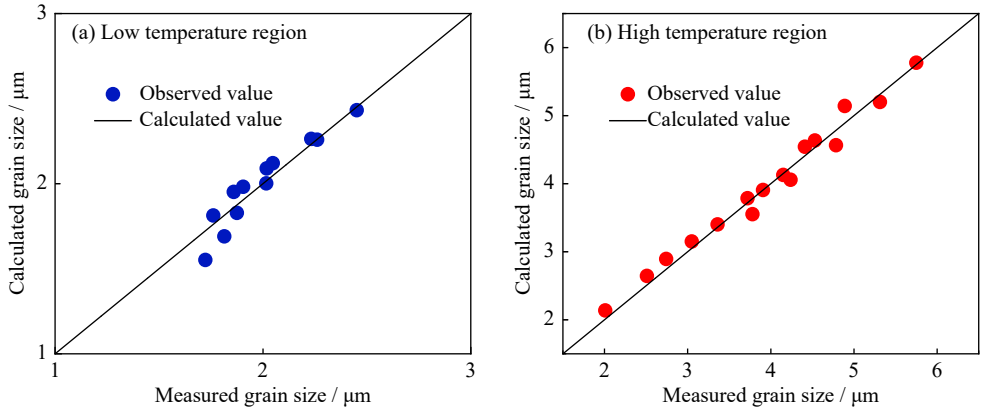

Fig. 11. Comparison of measured austenite grain size with calculated grain size during isothermal hold in (a) the low temperature region and (b) the high temperature region.

cording to the empirical formula Eqs. (7) and (8) [46]:

$$B_s = 745 - 110\omega_C - 59\omega_{Mn} - 39\omega_{Ni} - 68\omega_{Cr} - 106\omega_{Mo} + 17\omega_{Mn}\omega_{Ni} + 6\omega_{Cr}^2 + 29\omega_{Mo}^2 \quad (7)$$

$$M_s = 496.1(1 - 0.620\omega_C)(1 - 0.092\omega_{Mn})(1 - 0.033\omega_{Si})(1 - 0.045\omega_{Ni})(1 - 0.07\omega_{Cr})(1 - 0.029\omega_{Mo})(1 - 0.013\omega_W)(1 + 0.12\omega_{Co}) \quad (8)$$

where ω is the mass percent of elements in steel (the unit is %, and only numerical values are used for calculation). Based on the chemical composition of experimental steel, B_s and M_s are calculated to be 625.15°C and 373.85°C, respectively. After isothermal hold at different temperature for 1800 s, the solid phase transformation from austenite was observed *in situ* by CLSM during the continuous cooling process of strip cast sample. According to *in-situ* observation, the solid phase transformation in all samples took place in the range of 633–470.9°C. Obviously, the phase transformation during continuous cooling process belongs to bainite transformation.

Fig. 12 shows the typical *in-situ* pictures of bainite transformation in the strip samples held at different temperatures. The bainite transformation is closely related to nucleation positions, which can be divided into grain boundaries, phase interface, stacking fault, the free surface within grains [34–35]. Since there were almost no inclusions in the studied steel, the nucleation positions of bainites plates in this study are divided into three categories: at grain boundaries, within grain, on preformed bainite. In the previous study, non-lamellar cementite demonstrated the existence of carbon diffusion in the initiation of bainite transformation [47–48]. It can be seen that the bainite nucleated at austenite grain boundaries firstly, then nucleated within grain, and nucleated on preformed bainite plate finally (Fig. 12(a)–(d)). This is because the high energy of grain boundaries caused by irregular atomic arrangement and lattice distortion is conducive to carbon diffusion and bainite nucleation.

The growth rate of the bainite plates nucleating at different positions was also observed and measured by CLSM, as shown in Fig. 13. Fig. 13(d) shows the length variation of bainite plate marked in the Fig. 13(a)–(c) with time during the continuous cooling process after isothermal hold at 1350°C for 1800 s. It is indicated that the length of bainite plates is linear with time and the growth rate of the bainite plate marked by red circle is estimated to be 304.68 μm/s.

Using the same method, the growth rates of bainite plates nucleateing at different positions during continuous cooling process after isothermal hold at different temperature were measured and summarized in Table 2. The growth rate of the bainite plates in this work was calculated to be in range of 14.57 and 369.68 μm/s. Nutter *et al*. [49] has reported that the maximum velocity of ferrite/austenite interface migration in the Fe–C–Mn alloy is 0.5 μm/s, and it was calculated to be lower than 8 μm/s in the Fe–C alloy by Liu *et al*. [50].

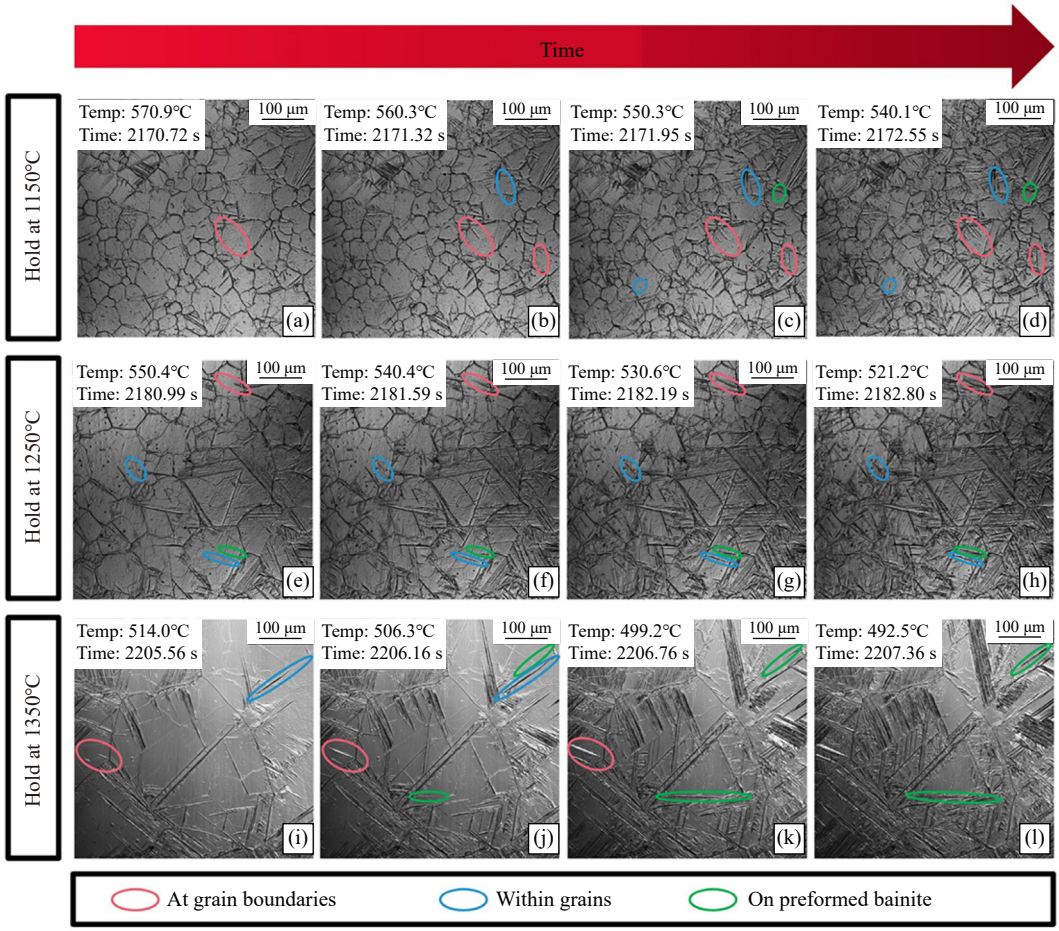

Fig. 12. Typical CLSM images of bainite transformation during continuous cooling process after isothermal hold at 1150 (a–d), 1250 (e–h), and 1350°C (i–l) for 1800 s.

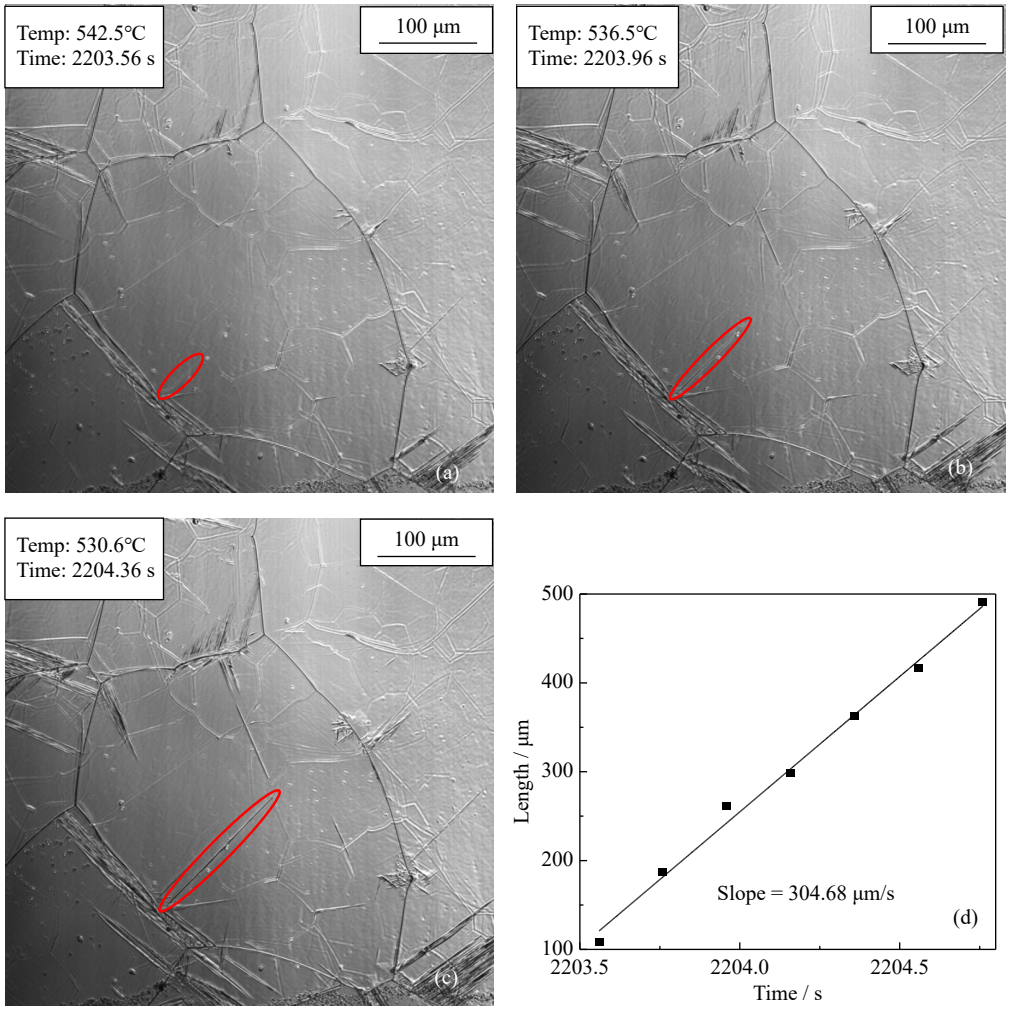

Fig. 13. (a–c) Growth process of the bainite plate nucleated at austenite grain boundary during continuous cooling process for the sample held at 1350°C for 1800 s and (d) the plot of bainite plate length versus time.

However, the average velocity of martensite/austenite interface migration in the Fe–Al alloy was calculated to be about 210 μm/s by Liu *et al*. [51]. Obviously, the growth rate of the bainite plates is much higher than that of ferrite and close to that of martensite. This is because the formation of bainite or martensite from austenite belongs to displacive phase transformation, which is different with the diffusional phase transformation of ferrite from austenite. It also can be found from Table 2 that the average growth rate of the bainite plates nucleating at grain boundaries is the highest and the average growth rate of the bainite plates nucleating on preformed bainite plate is the lowest. It can be attributed to two reasons. At first, the bainite plates nucleating at grain boundaries grew at a higher temperature, which promoted the diffusion of carbon element and thus led to a higher growth rate of bainite plates due to the diffused characteristics of bainite transformation. Besides, more vacancies and dislocations at grain boundaries can act as the channels for carbon diffusion, which also promote the growth of the bainite plates nucleating at grain boundaries. However, the formation of bainite

Table 2. Summary of growth rates of the bainite plates under different conditions

Holding temperature / °C	Nucleation position	Lath growth rate / (μm·s^{-1})		
		Maximum	Minimum	Average
1150	At grain boundaries	188.08	60.52	138.47
	Within grain	152.41	34.26	81.93
	On preformed bainite plates	107.11	14.57	55.34
1250	At grain boundaries	291.77	54.56	169.93
	Within grain	154.30	70.90	115.46
	On preformed bainite plates	116.35	55.45	80.81
1350	At grain boundaries	369.68	88.55	180.82
	Within grain	250.70	42.56	143.64
	On preformed bainite plates	287.82	41.59	117.86

ferrite increases the carbon content in the surrounding austenite, and thus increases the stability of austenite, which inhibit the growth of the bainite plates nucleating in the preformed bainite plates.

As shown in Fig. 6, the grain size of austenite during isothermal hold process is positively correlated with holding temperature. Fig. 14 summarizes the average value and the standard deviation of the growth rates of the bainite plates nucleating at different positions during continuous cooling process after isothermal hold. It is indicated that the growth

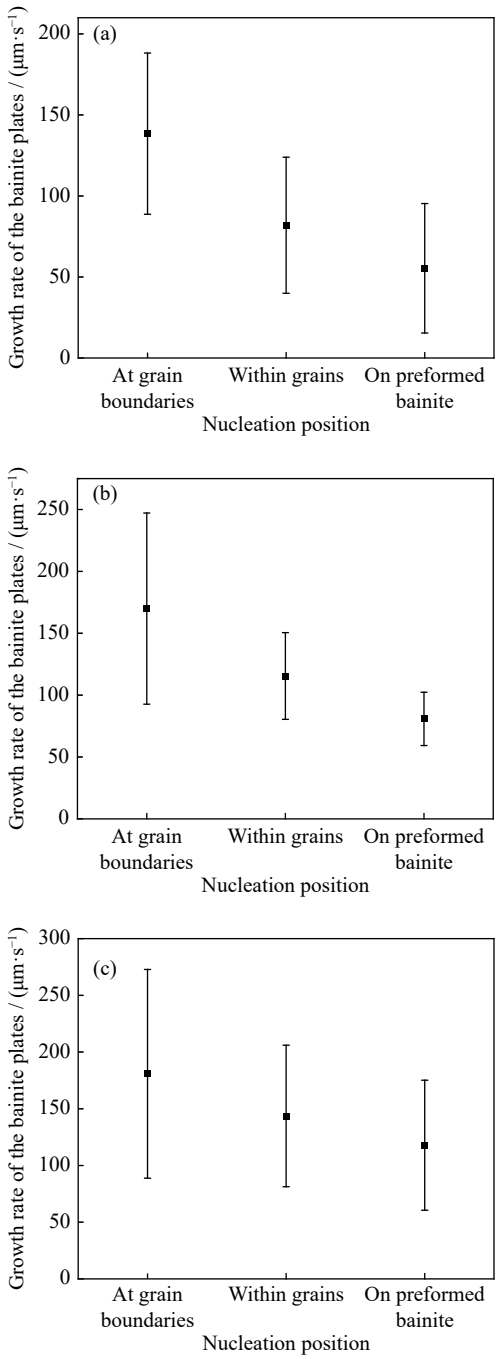

Fig. 14. Growth rates of the bainite plates nucleating at grain boundaries, within grains and on preformed bainite during continuous cooling process after isothermal hold at 1150 (a), 1250 (b), and 1350°C (c) for 1800 s. Error bar represents standard deviation.

rates of bainite plates in coarse austenite grain is higher than that in fine austenite grain. It has been demonstrated that the carbon and manganese elements would easily gather at the austenite grain boundaries during the continuous cooling process when the temperature is higher than austenite formation temperature [52]. Compared with coarse austenite grain, the migrated distance of the carbon and manganese elements in fine austenite grain is shorter, leading to a more serious segregation at grain boundaries. The segregation would enhance the stability of austenite, thus reduce the growth rate of bainite plates nucleating at the austenite grain boundaries. Meanwhile, previously formed bainite plates in fine austenite grain provide more resistance for the growth of bainite plates than coarse austenite grain. Therefore, the overall growth rate of bainite plates in fine austenite grain is lower than that in coarse austenite grain.

The bainite fraction of 95% was deemed as the end of bainite transformation. The relationship between bainite transformation fraction versus transformation time during continuous cooling process after isothermal hold at different temperature for 1800 s is shown in Fig. 15. It can be seen that the time required for bainite transformation completion is 6.6, 7.2, and 6.6 s after isothermal hold at 1150, 1250, and 1350°C for 1800 s, respectively. Therefore, although the average growth rate of single bainite plate in coarse austenite grain is faster than that in fine austenite grain, the overall bainite transformation rate of strip cast during continuous cooing after the isothermal hold at different temperatures are similar each other. This is because the fine austenite grain structure has more nucleation positions on grain boundaries and therefore can produce more bainite plates at the same time, as shown in Fig. 12.

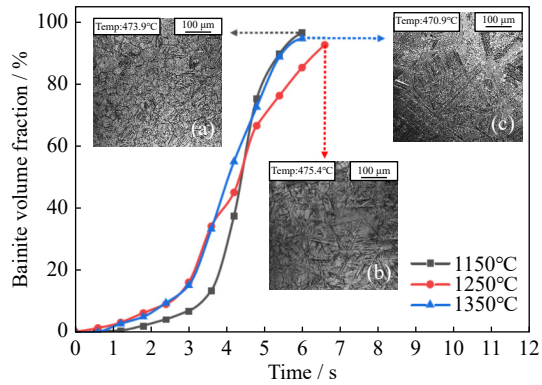

Fig. 15. Relationship of bainite transformation volume fraction and transformation time during continuous cooling process after isothermal hold at different temperature for 1800 s and the images of bainite transformation completion after isothermal hold at 1150°C (a), 1250°C (b), and 1350°C (c) for 1800 s.

4. Conclusions

The austenite growth and bainite transformation during the reheating and continuous cooling processes of microalloyed steel produced by simulated strip casting were ob-

served *in situ* by CLSM for the first time. Then the kinetics of austenite isothermal growth and bainite transformation were investigated, and the conclusions were drawn as follows.

(1) When the holding temperature below 1000°C, the austenite grains of the microalloyed steel strip produced by simulated strip casting grew slowly during the reheating treatment, due to the inhibition of austenite grain growth by small-size second phase particles like NbC and TiC. The kinetics model of austenite isothermal growth during the isothermal hold of the microalloyed steel strip was deduced as $D^{1/0.06} - D_0^{1/0.06} = 3.001 \times 10^{43} \exp\left(-6.932 \times \frac{10^5}{RT}\right) t$ ($T < 1273$ K) and $D^{1/0.22} - D_0^{\frac{1}{0.22}} = 2.996 \times 10^{25} \exp\left(-5.38 \times \frac{10^5}{RT}\right) t$ ($T \geq 1273$ K).

(2) The precipitation behavior of second phase particle was significantly affected by the holding temperature. The particles precipitated at low temperature region (<1000°C) was fine and high-density, which can inhibit the growth of austenite grains well. With the increasing of holding temperature, the particles become coarse and the number density of particles decreases. The activation energy for austenite grain growth during the isothermal hold of the microalloyed steel strip produced by strip casting was calculated to be 538.0 and 693.2 kJ/mol in the high temperature region and low temperature region, respectively.

(3) During bainite transformation, nucleation took place at grain boundaries firstly, then within grains, and finally on the preformed bainite. The average growth rate of the bainite plates nucleating at grain boundaries was the fastest and that on preformed bainite plate is the lowest. The growth rate of bainite plates is also related to austenite grain size and the bainite plates grow faster in coarse austenite grain. However, the overall bainite transformation rate is similar for different holding temperature in spite of different austenite grain size.

Acknowledgements

The study was financially supported from the National Natural Science Foundation of China (No. 52130408), the Hunan Scientific Technology Project, China (Nos. 2019RS3007 and 2020WK2003), and the Fundamental Research Funds for the Central Universities of Central South University, China.

Conflict of Interest

The authors have no relevant financial or non-financial interests to disclose.

References

[1] X.D. Huo, J.N. Xia, L.J. Li, Z.W. Peng, S.J. Chen, and C.T. Peng, A review of research and development on titanium microalloyed high strength steels, *Mater. Res. Express*, 5(2018), No. 6, art. No. 062002.

[2] T.N. Baker, Microalloyed steels, *Ironmaking Steelmaking*, 43(2016), No. 4, p. 264.

[3] A. Zaitsev and N. Arutyunyan, Low-carbon Ti–Mo microalloyed hot rolled steels: Special features of the formation of the structural state and mechanical properties, *Metals*, 11(2021), No. 10, art. No. 1584.

[4] Y. Liu, Y.H. Sun, and H.T. Wu, Effects of chromium on the microstructure and hot ductility of Nb-microalloyed steel, *Int. J. Miner. Metall. Mater.*, 28(2021), No. 6, p. 1011.

[5] Y.N. Zhao, Z.Q. Ma, L.M. Yu, J. Dong, and Y.C. Liu, The simultaneous improvements of strength and ductility in additive manufactured Ni-based superalloy via controlling cellular subgrain microstructure, *J. Mater. Sci. Technol.*, 68(2021), p. 184.

[6] L. Yang, Y. Li, Z.L. Xue, and C.G. Cheng, Effect of different thermal schedules on ductility of microalloyed steel slabs during continuous casting, *Metals*, 9(2019), No. 1, art. No. 37.

[7] S.K. Giri, T. Chanda, S. Chatterjee, and A. Kumar, Hot ductility of C–Mn and microalloyed steels evaluated for thin slab continuous casting process, *Mater. Sci. Technol.*, 30(2014), No. 3, p. 268.

[8] J. Zhou, Y.L. Kang, and X.P. Mao, Precipitation characteristic of high strength steels microalloyed with titanium produced by compact strip production, *J. Univ. Sci. Technol. Beijing*, 15(2008), No. 4, p. 389.

[9] N. Zapuskalov, Comparison of continuous strip casting with conventional technology, *ISIJ Int.*, 43(2003), No. 8, p. 1115.

[10] S. Ge, M. Isac, and R.I.L. Guthrie, Progress of strip casting technology for steel; historical developments, *ISIJ Int.*, 52(2012), No. 12, p. 2109.

[11] S. Ge, M. Isac, and R.I.L. Guthrie, Progress in strip casting technologies for steel; technical developments, *ISIJ Int.*, 53(2013), No. 5, p. 729.

[12] A. Maleki, A. Taherizadeh, and N. Hosseini, Twin roll casting of steels: An overview, *ISIJ Int.*, 57(2017), No. 1, p. 1.

[13] J.Y. Heo, M.S. Baek, K.J. Euh, and K.A. Lee, Microstructure, tensile and fatigue properties of Al–5wt.%Mg alloy manufactured by twin roll strip casting, *Met. Mater. Int.*, 24(2018), No. 5, p. 992.

[14] Y. Kwon, J.H. Hwang, H.C. Choi, *et al.*, Microstructure and tensile properties of ferritic lightweight steel produced by twin-roll casting, *Met. Mater. Int.*, 26(2020), No. 1, p. 75.

[15] R. Wechsler, The status of twin-roll casting technology, *Scand. J. Metall.*, 32(2003), No. 1, p. 58.

[16] M. Ferry, *Direct Strip Casting of Metals and Alloys*, Woodhead Publishing, Cambridge, 2006.

[17] Z.P. Xiong, A.G. Kostryzhev, N.E. Stanford, and E.V. Pereloma, Effect of deformation on microstructure and mechanical properties of dual phase steel produced via strip casting simulation, *Mater. Sci. Eng. A*, 651(2016), p. 291.

[18] Z.P. Xiong, A.G. Kostryzhev, N.E. Stanford, and E.V. Pereloma, Microstructures and mechanical properties of dual phase steel produced by laboratory simulated strip casting, *Mater. Des.*, 88(2015), p. 537.

[19] Z.P. Xiong, A.G. Kostryzhev, A.A. Saleh, L. Chen, and E.V. Pereloma, Microstructures and mechanical properties of TRIP steel produced by strip casting simulated in the laboratory, *Mater. Sci. Eng. A*, 664(2016), p. 26.

[20] Z.P. Xiong, A.G. Kostryzhev, L. Chen, and E.V. Pereloma, Microstructure and mechanical properties of strip cast TRIP steel subjected to thermo-mechanical simulation, *Mater. Sci. Eng. A*, 677(2016), p. 356.

[21] M.J. Ha, W.S. Kim, H.K. Moon, B.J. Lee, and S. Lee, Analysis and prevention of dent defects formed during strip casting of twin-induced plasticity steels, *Metall. Mater. Trans. A*, 39(2008), No. 5, p. 1087.

[22] M. Daamen, W. Nessen, P.T. Pinard, S. Richter, A. Schwedt, and G. Hirt, Deformation behavior of high-manganese TWIP steels produced by twin-roll strip casting, *Procedia Eng.*,

81(2014), p. 1535.
[23] S.L. Shrestha, K.Y. Xie, C. Zhu, *et al*., Cluster strengthening of Nb-microalloyed ultra-thin cast strip steels produced by the CASTRIP® process, *Mater. Sci. Eng. A*, 568(2013), p. 88.
[24] K.Y. Xie, T.X. Zheng, J.M. Cairney, *et al*., Strengthening from Nb-rich clusters in a Nb-microalloyed steel, *Scripta. Mater.*, 66(2012), No. 9, p. 710.
[25] L. Xu, J. Shi, W.Q. Cao, M.Q. Wang, W.J. Hui, and H. Dong, Improved mechanical properties in Ti-bearing martensitic steel by precipitation and grain refinement, *J. Mater. Sci.*, 46(2011), No. 19, p. 6384.
[26] L. Xu, J. Shi, W.Q. Cao, M.Q. Wang, W.J. Hui, and H. Dong, Yield strength enhancement of martensitic steel through titanium addition, *J. Mater. Sci.*, 46(2011), No. 10, p. 3653.
[27] Y. Han, J. Shi, L. Xu, W.Q. Cao, and H. Dong, Effect of hot rolling temperature on grain size and precipitation hardening in a Ti-microalloyed low-carbon martensitic steel, *Mater. Sci. Eng. A*, 553(2012), p. 192.
[28] M.A. Hafeez, A. Farooq, K.B. Tayyab, and M.A. Arshad, Effect of thermomechanical cyclic quenching and tempering treatments on microstructure, mechanical and electrochemical properties of AISI 1345 steel, *Int. J. Miner. Metall. Mater.*, 28(2021), No. 4, p. 688.
[29] G.W. Yang, X.J. Sun, Z.D. Li, X.X. Li, and Q.L. Yong, Effects of vanadium on the microstructure and mechanical properties of a high strength low alloy martensite steel, *Mater. Des.*, 50(2013), p. 102.
[30] G.W. Yang, Z.D. Li, X.J. Sun, X. Yong, and Q.L. Yong, Ultrafine grained austenite in a low carbon vanadium microalloyed steel, *J. Iron Steel Res. Int.*, 20(2013), No. 4, p. 64.
[31] P.A. Manohar, D.P. Dunne, T. Chandra, and C.R. Killmore, Grain growth predictions in microalloyed steels, *ISIJ Int.*, 36(1996), No. 2, p. 194.
[32] J. Moon, J. Lee, and C. Lee, Prediction for the austenite grain size in the presence of growing particles in the weld HAZ of Ti-microalloyed steel, *Mater. Sci. Eng. A*, 459(2007), No. 1-2, p. 40.
[33] G.W. Yang, X.J. Sun, Q.L. Yong, Z.D. Li, and X.X. Li, Austenite grain refinement and isothermal growth behavior in a low carbon vanadium microalloyed steel, *J. Iron Steel Res. Int.*, 21(2014), No. 8, p. 757.
[34] Y. Shen, B. Chen, and C. Wang, *In situ* observation and growth kinetics of bainite laths in the coarse-grained heat-affected zone of 2.25Cr–1Mo heat-resistant steel during simulated welding, *Metall. Mater. Trans. A*, 52(2021), No. 1, p. 14.
[35] Z.W. Hu, G. Xu, H.J. Hu, L. Wang, and Z.L. Xue, *In situ* measured growth rates of bainite plates in an Fe–C–Mn–Si superbainitic steel, *Int. J. Miner. Metall. Mater.*, 21(2014), No. 4, p. 371.
[36] P.S. Lyu, W.L. Wang, H.R. Qian, J.C. Wu, and Y. Fang, Formation of naturally deposited film and its effect on interfacial heat transfer during strip casting of martensitic steel, *JOM*, 72(2020), No. 5, p. 1910.
[37] P.S. Lyu, W.L. Wang, C.H. Wang, L.J. Zhou, Y. Fang, and J.C. Wu, Effect of sub-rapid solidification and secondary cooling on microstructure and properties of strip cast low-carbon bainitic–martensitic steel, *Metall. Mater. Trans. A*, 52(2021), No. 9, p. 3945.
[38] W.L. Wang, H.R. Qian, D.W. Cai, L.J. Zhou, S. Mao, and P.S. Lyu, Microstructure and magnetic properties of 6.5 wt pct Si steel strip produced by simulated strip casting process, *Metall. Mater. Trans. A*, 52(2021), No. 5, p. 1799.
[39] S.J. Yao, L.X. Du, X.H. Liu, G.D. Wang, Isothermal growth kinetics of ultra-fine austenite grains in a Nb–V–Ti microalloyed steel, *J. Mater. Sci. Technol.*, 25(2009), No. 5, p. 615.
[40] H. Hu and B.B. Rath, On the time exponent in isothermal grain growth, *Metall. Trans.*, 1(1970), No. 11, p. 3181.
[41] S. Gündüz and R.C. Cochrane, Influence of cooling rate and tempering on precipitation and hardness of vanadium microalloyed steel, *Mater. Des.*, 26(2005), No. 6, p. 486.
[42] L.J. Li and R.W. Messler, Dissolution kinetics of NbC particles in the heat-affected zone of type 347 austenitic stainless steel, *Metall. Mater. Trans. A*, 33(2002), No. 7, p. 2031.
[43] F.J. Ma, G.H. Wen, P. Tang, G.D. Xu, F. Mei, and W.L. Wang, Effect of cooling rate on the precipitation behavior of carbonitride in microalloyed steel slab, *Metall. Mater. Trans. B*, 42(2011), No. 1, p. 81.
[44] K.Y. Tsai, M.H. Tsai, and J.W. Yeh, Sluggish diffusion in Co–Cr–Fe–Mn–Ni high-entropy alloys, *Acta Mater.*, 61(2013), No. 13, p. 4887.
[45] S. Uhm, J. Moon, C. Lee, J. Yoon, and B. Lee, Prediction model for the austenite grain size in the coarse grained heat affected zone of Fe–C–Mn steels: Considering the effect of initial grain size on isothermal growth behavior, *ISIJ Int.*, 44(2004), No. 7, p. 1230.
[46] J.Y. Tian, G. Xu, L. Wang, M.X. Zhou, and H.J. Hu, *In situ* observation of the lengthening rate of bainite sheaves during continuous cooling process in a Fe–C–Mn–Si superbainitic steel, *Trans. Indian Inst. Met.*, 71(2018), No. 1, p. 185.
[47] L. Fielding, The bainite controversy, *Mater. Sci. Technol.*, 29(2013), p. 383.
[48] Z.X. Qiao, Y.C. Liu, L.M. Yu, and Z.M. Gao, Formation mechanism of granular bainite in a 30CrNi$_3$MoV steel, *J. Alloys Compd.*, 475(2009), No. 1-2, p. 560.
[49] J. Nutter, H. Farahani, W.M. Rainforth, and S. van der Zwaag, Direct TEM observation of α/γ interface migration during cyclic partial phase transformations at intercritical temperatures in an Fe–0.1C −0.5Mn alloy, *Acta Mater.*, 178(2019), p. 68.
[50] Y.C. Liu, D.J. Wang, F. Sommer, and E.J. Mittemeijer, Isothermal austenite–ferrite transformation of Fe–0.04 at.% C alloy: Dilatometric measurement and kinetic analysis, *Acta Mater.*, 56(2008), No. 15, p. 3833.
[51] Y.C. Liu, L.F. Zhang, F. Sommer, and E.J. Mittemeijer, Kinetics of martensite formation in substitutional Fe–Al alloys: Dilatometric analysis, *Metall. Mater. Trans. A*, 44(2013), No. 3, p. 1430.
[52] X.D. Li, C.J. Shang, X.P. Ma, *et al*., Elemental distribution in the martensite–austenite constituent in intercritically reheated coarse-grained heat-affected zone of a high-strength pipeline steel, *Scripta. Mater.*, 139(2017), p. 67.